RSC Sustainability

ROYAL SOCIETY OF CHEMISTRY

PAPER

View Article Online
View Journal | View Issue

Cite this: *RSC Sustainability*, 2024, **2**, 1515

GQD-PAN-based high-performance supercapacitor: an approach towards wealth from waste†

Dheeraj Kumar,[a] Ekta Vashishth,[a] Sweety Rani,[a] Advitiya Kumar,[a] Bhanu Nandan,[a] Supreet Singh Bahga[b] and Rajiv K. Srivastava *[a]

Managing non-biodegradable polymeric waste and exploring efficient energy materials are imperative and need immediate attention. Herein, these two highly demanding problems were solved simultaneously by synthesizing nonpolar graphene quantum dots (GQDs) from non-biodegradable plastic waste and using the GQDs to fabricate energy storage systems. The GQDs were synthesized using styrofoam waste and coated on a carbonized polyacrylonitrile electrospun matrix (cPAN) to fabricate three- and two-electrode supercapacitors. A GQD coating of 0.4 mg led to an areal capacitance of 1883 mF cm^{-2} (or a volumetric capacitance of 784 F g^{-1}) at 2 mA cm^{-2} in a three-electrode supercapacitor, which was ~78 times the capacitance produced in neat cPAN. The energy density also increased from 4 to 316.5 μW h cm^{-2} compared to neat cPAN. In addition, the two-electrode supercapacitor exhibited high capacitance, energy density and power density values of 59.7 mF cm^{-2}, 10 μW h cm^{-2} and 125 μW cm^{-2}, respectively. Additionally, both the three- and two-electrode supercapacitors maintained their capacitive behaviour for three thousand charge–discharge cycles. Thus, the approach developed in this work for the synthesis of efficient energy storage materials can be expanded to other plastic wastes for the generation of value-added products and unexplored applications, while addressing pertinent issues related to the environment.

Received 27th March 2024
Accepted 2nd April 2024

DOI: 10.1039/d4su00153b

rsc.li/rscsus

Sustainability spotlight

This study emphasizes the importance of ensuring sustainable consumption and production patterns (SDG 12 of the UN). The pollution due to plastic waste as solids or emissions in the aquatic and terrestrial ecosystem and the UN's aim of mitigating their detrimental consequences on human well-being and the environment as stipulated in SDG 12 are addressed in the present work through the process of recycling plastic waste into advanced nanomaterials. Subsequently, these nanomaterials are harnessed for energy storage applications, ensuring access to affordable, reliable, sustainable, and modern energy for all (SDG 7). The conversion of plastic waste into quantum dots, followed by their utilization in energy storage applications can contribute to universal access to affordable, reliable, and state-of-the-art energy services while minimizing the adverse effect of plastic waste.

1. Introduction

The past decade has witnessed an increase in the demand for new energy storage devices and related technologies to overcome the serious energy crisis imposed by the depletion of natural sources.[1] Thus, efforts have been devoted to finding new materials for energy storage devices that can outperform the current generation of materials. Batteries have long been the conventional energy storage devices of choice, offering relatively high energy density and long-lasting power. However, they often suffer from limitations in terms of charging time and lifespan. Alternatively, electrochemical capacitors, also known as supercapacitors, seem to fulfil future energy storage device requirements because of their miniaturised size, portability and fast charging–discharging at a high power density.[2,3] The field of energy storage has experienced remarkable advancement, propelled by the escalating demands for efficient and sustainable solutions. Noteworthy progress has been achieved in sulfur composite battery research,[4–6] wherein innovative metal–air batteries[7] have led to a demonstrably extended lifespan. On the supercapacitor frontier, GQDs,[8–10] MXenes,[11–13] carbon composites,[14] metal–organic frameworks (MOFs),[15,16] and conducting polymers[17] have emerged as promising candidates, facilitating the fabrication of high-performance devices with exceptional rate capabilities. With the escalating demand for sustainable energy solutions, continued exploration and

[a]*Department of Textile and Fibre Engineering, Indian Institute of Technology Delhi, Hauz Khas, New Delhi 110016, India. E-mail: rajiv@iitd.ac.in*

[b]*Department of Mechanical Engineering, Indian Institute of Technology Delhi, Hauz Khas, New Delhi 110016, India*

† Electronic supplementary information (ESI) available. See DOI: https://doi.org/10.1039/d4su00153b

innovation in these domains are imperative for the development of next-generation energy storage technologies. Studies have explored the utilization of both biodegradable[18–21] and non-biodegradable[22,23] waste materials in energy storage applications. The investigation of supercapacitor active materials from non-biodegradable plastic waste has been driven by the urgent need for sustainable energy solutions. In this case, supercapacitors play an important role as we move from limited natural resources to renewable energy sources for different applications, including electric vehicles and energy production powerplants. Depending on the energy storage mechanism, electrochemical double-layer capacitors (EDLCs) and pseudocapacitors are the two classes of supercapacitors that store energy at the electrode–electrolyte interface and faradaic reversible reactions of electroactive materials, respectively. Given that the capacitance and performance of EDLCs mainly depend on the electrode material, the search for materials with a high surface to volume ratio, electrode compatibility, and good conductivity for supercapacitors is necessary despite the easy availability of a wide range of electrode materials.[24]

Carbon nanomaterials have high potential to overcome the challenging demands of supercapacitors due to their tuneable conductivity and ultra-high surface area. Carbonaceous materials with a high conductivity, specific surface area and low fabrication cost are desirable as electrochemical double layer (EDL) active materials for supercapacitors. In this case, carbon quantum dots,[25–32] carbon nano-onions,[33–37] graphene,[38–42] and porous carbon composites[43–50] have become a focus of research in the energy device sector. This is ascribed to their unique structural properties and marginal change in mechanical, thermal and electrical properties given that all atoms are utilised to contribute to these properties.

Among the carbon nanoforms, zero-dimensional graphene quantum dots (GQDs) are one of the most exciting nanomaterials because of their high quantum confinement, which opens up new extraordinary properties that have never been seen before. GQDs without doping,[51–55] doped GQDs,[56–60] and GQD composites[61–64] have been explored as EDL materials, and it has been found that they exhibit good specific capacitance values at a high current density. The sp^2 hybridized single-layer carbon hexagons with pie-electron cloud in GQDs give rise to higher conductivity, which contributes to further increasing the capacitance. However, the synthesis of GQDs involves the use of harsh acids or bases, which create defects in the continuous sp^2 hybridization and hamper their innate properties. Thus, the production of defect-free zero-dimensional nanomaterials typically requires costly precursors and technology. Energy-related materials provide multi-fold benefits if produced from non-biodegradable plastic waste or other environmental pollutants.

The reuse and recycling of plastic are two conventional ways to mitigate the environmental concerns raised by plastic debris. This paves a plausible route for realizing a circular economy; however, the formation of value-added products, especially for the energy sector, from these non-degradable wastes, which typically converge as landfill or sewage is challenging. In this case, carbon quantum dots (CQDs) with luminescence behaviour, low toxicity, biocompatibility, good conductivity and stability have attracted attention from researchers worldwide, especially their synthesis from different types of waste. CQDs have been synthesized using waste from the paper,[65] plastic[66,67] and food industries.[68–71] Most of these techniques involve first the conversion of waste into bulk carbon form *via* thermal energy, and then converting the bulk carbon form into a quantum size using harsh basic or acidic conditions. The use of base or acids in these methods leads to the generation of different types of polar functional groups on the surface of CQDs, which further limit their applications and compatibility with other carbon forms. Thus, it is necessary to search for nonpolar CQDs for carbon electrode-based applications given that they show higher compatibility with other nonpolar carbon electrodes, and ultimately may lead to a significant enhancement in the desired properties.[72]

In this work, supercapacitor electrodes were fabricated using a nonpolar GQD-coated carbonized polyacrylonitrile electrospun matrix (cPAN) to achieve a superior capacitance. Nonpolar GQDs were synthesized using our previously reported method, in which non-biodegradable Styrofoam waste was pyrolyzed under microwave radiation in an acid/base/catalyst-free environment.[73] Nonpolar GQDs have the advantage of high compatibility with other nonpolar carbon materials.[72] The contact angle of water on cPAN fibre increased from 137° to 145° after coating GQDs (shown in Fig. S1†), which showed the good compatibility of the nonpolar GQDs with the cPAN matrix. It is established that nonpolar carbon materials demonstrate enhanced compatibility with other carbon materials with a nonpolar nature. This observation underscores the favourable interaction between the GQDs and the carbonized PAN substrate, further supporting the compatibility of GQDs for integration with the electrode material. The electrochemical analysis was performed by fabricating three- and two-electrode systems composed of the GQD-coated cPAN matrix. The GQD-coated cPAN, platinum sheet and Ag/AgCl were used as the working, counter and reference electrodes, respectively, in the three-electrode system. Moreover, a coin cell-based two-electrode system was also fabricated using GQD-coated cPAN, cotton fabric and neat cPAN as the cathode, separator, and anode, respectively. This work was focused on developing a value-added, novel and inexpensive product using non-biodegradable plastic waste in the form of quantum dots to achieve exceptional capacitance properties in the corresponding fabricated supercapacitors.

2. Experimental

2.1. Materials

Styrofoam waste was collected from the packaging boxes of home appliances, having a weight-average molecular weight (M_w) and number-average molecular weight (M_n) of 108 035 and 43 811, respectively. The Ag/AgCl/KCl saturated reference electrode was purchased from Biologic Science Instruments, India. The coin cell holder assembly was purchased from a local vendor. Whatman filter paper with a diameter of 125 mm and pore size of 11 μm was used for filtration. Chloroform, toluene,

dimethylformamide (DMF) and sulfuric acid of SQ grade were purchased from Fischer Scientific. All chemicals were used as received without any further purification or modification.

2.2. Synthesis of GQDs

Our previously reported method was employed for the synthesis of GQDs from Styrofoam waste.[73] Briefly, the air in the waste Styrofoam was squeezed out by dissolving it in chloroform to avoid the formation of carbon oxide gases. A Rota-evaporator was used to recover the chloroform and a solid mass of Styrofoam was formed after the evaporation of the chloroform. The solid mass of 0.5 ± 0.01 g was treated at 370 °C for 30 min at a ramping rate of 10 °C min^{-1} in a microwave furnace. The as-obtained dark brown color residue was dispersed in toluene and filtered using Whatman filter paper to separate the bulk impurities. The synthesis was performed in triplicate to check the reproducibility of the process and as-obtained product. The GQD toluene colloidal solution was further used for the fabrication of the supercapacitor electrodes.

2.3. Preparation of carbonized electrospun PAN matrix

Electrospinning was used to prepare the PAN-based carbon nanofibres. Briefly, a PAN (9% wt/wt) solution was made in DMF and kept under magnetic stirring for 24 h. The resulting polymer solution was electrospun using an electrospinning setup (E-Spin Nanotech, India) at an applied voltage of 18 kV and feeding rate of 1 mL h^{-1}. The distance from the tip to the collector was fixed at 21 cm. The electrospun nanofibres were stabilized at 250 °C for 90 min in the presence of air, followed by carbonization at 750 °C for 2 h in a nitrogen atmosphere. The electrospun carbonized PAN matrix was prepared in triplicate to check the reproducibility.

2.4. Fabrication of three- and two-electrode based supercapacitors

The working electrode of the supercapacitor was prepared by cutting the cPAN matrix to a size of 1 cm^2. The cut matrix was connected with a 0.38 mm diameter copper wire using silver paste. Subsequently, the prepared electrode was inserted into a glass pipe with a diameter of 6 mm and glued with epoxy resin and dried in an oven at 40 °C for 12 h. The final cPAN matrix electrodes were dipped into two different concentration GQD toluene colloidal solutions for 12 h and dried in an oven for an additional 12 h at 50 °C. A weight gain of 0.1 and 0.4 mg was observed on the cPAN matrices after the dipping and drying process for the two different concentration GQD toluene colloidal solutions, respectively. The electrodes were used as working electrodes for further electrochemical characterization. A platinum sheet with the dimensions of 2.5 cm × 1.5 cm × 0.014 cm was used to prepare the counter electrode using the same procedure with silver paste and epoxy resin. Ag/AgCl and 1 M H_2SO_4 were used as the reference electrode and electrolyte, respectively. All the electrodes were fitted into a Teflon-capped glass cell to form a three-electrode-based supercapacitor, as shown in Fig. S7.†

In the case of the coin cell-based two-electrode system, the cPAN matrix and cotton cloth were calendared and punched into a circular shape with a diameter of 15 mm. The cut cPAN circular electrode was dipped into the GQD colloidal solution and the final GQD coating weight after drying was measured (0.1 mg). The GQD-coated cPAN was used as the cathode. Neat cPAN and cotton were used as the anode and separator in the fabrication process, respectively. The cathode, anode and separator were dipped into 1 M H_2SO_4 electrolyte solution. A spacer was also used in the assembly to avoid any unwanted connection and realize the uniform contact of the electrodes with the current collector. Finally, the coin cell-based assembly was used for all the two-electrode-based electrochemical characterizations. The two- and three-electrode fabrication process was repeated to produce three replicates to check their reproducibility in terms of capacitance behaviour.

2.5. Areal capacitance calculations

The area capacitance (C) was calculated from GCD using eqn (1), where I (mA cm^{-2}) is the current density, Δt (s) is the discharge time, S (cm^2) is the effective area, and ΔV (V) is the potential window.

$$C\ (\mathrm{mF\ cm^{-2}}) = \frac{I \times \Delta t}{S \times \Delta V} \quad (1)$$

The energy density (E) and power density (P) were calculated from eqn (2) and (3), respectively.

$$E(\mu\mathrm{W\ h\ cm^{-2}}) = \frac{1}{7.2} \times C \times (\Delta V)^2 \quad (2)$$

$$P(\mu\mathrm{W\ cm^{-2}}) = \frac{E}{t} \times 3600 \quad (3)$$

2.6. Characterization and equipment

The transmission electron microscopy (TEM) images of the coated and neat cPAN matrix were recorded on a FEI Tecnai TF20 at 200 kV. The GQD-coated and neat cPAN matrix samples were crushed using an electric mixture and sonicated in toluene to prepare a TEM copper grid with a mesh size of 300. XPS (X-ray photoelectron spectroscopy) was performed using a Kratos Analytical Limited AXIS Supra instrument. The samples were analyzed by Horiba Raman spectroscopy using a 325 nm laser at a power of 12.5 mW. Nitrogen sorption measurements were performed using a BELSORP-miniX instrument. All the samples were degassed at 50 °C for 6 h and their surface area was calculated using the BET (Brunauer–Emmett–Teller) method. Electrochemical measurements were performed in a three-electrode system on a VMP3 BioLogic Science Instruments.

3. Results and discussion

According to our previous report,[53] GQDs were synthesized *via* the microwave-assisted pyrolysis of waste Styrofoam and electrospun PAN fibres were carbonized for the fabrication of

supercapacitor electrodes. The GQD samples and electrodes with their replicas were further characterized using advanced analytical instruments including electrochemical studies. The neat cPAN and GQD-coated cPAN fibres were partially crushed using a mortar-pestle and dispersed in ethanol *via* sonication for the preparation of the transmission electron microscopy (TEM) grids. The high-resolution TEM images in Fig. 1A confirm the presence of cPAN fibres with a diameter of around 300 nm, while in the case of the GQD dip-coated cPAN fibres (Fig. 1B), the adequate deposition of GQDs was confirmed on the fibres. The size distribution of the GQDs was determined to be 6 ± 1.5 nm based on the analysis of the TEM images, as depicted in Fig. S5.† The high-resolution image of GQDs inserted in Fig. 1B confirms the presence of uniform circular-shape GQDs, as also reported in our previous study.

X-ray photoelectron spectroscopy (XPS) was also performed for both the neat cPAN and GQD-coated cPAN matrix, as shown in Fig. 2A and B, respectively. In the neat cPAN fibre, a nitrogen peak was seen at 398 eV. In contrast, no nitrogen peak was observed in the case of the GQD-coated cPAN. Moreover, the high-resolution carbon 1s spectrum was also recorded to confirm the presence of carbon–nitrogen (C–N) and carbon–oxygen (C=O) functionalities in both samples. No peaks were observed for C–N and C=O in the GQD-coated sample, which confirmed the surface deposition of GQDs throughout the cPAN fibre. However, after deconvolution, the appearance of peaks at 285.5 and 288.3 eV confirmed the presence of C–N and C=O functionalities in the neat cPAN samples coming from the carbonization of polyacrylonitrile in the presence of oxygen, respectively.[74] A peak for the carbon–oxygen (C=O) functionality at 533 eV was also observed in both samples, which may have originated from the oxidation process of PAN fibre.[75] Hence, the absence of nitrogen functionalities according to XPS in the GQD-coated cPAN fibred confirmed the uniform coating of GQDs over the cPAN fibres.

Fig. 3A and B show the Raman spectra of the neat cPAN and GQD-coated cPAN fibres used for the fabrication of the supercapacitor, respectively. Both samples were analysed at an exposure time of three seconds with five accumulations using a 325 nm laser at a power of 12.5 mW. A higher intensity defect band (1350 cm^{-1}) was observed in the case of the neat cPAN fibres compared to the GQD-coated cPAN fibres, indicating the presence of a higher number of defects in neat cPAN compared to the GQD-coated cPAN. In the case of the graphitic band (1597 cm^{-1}), lesser broadening was observed for GQD-coated cPAN, which indicated a more uniform graphitic structure compared to neat cPAN.[76,77] The I_d/I_g ratios were also calculated to be 0.36 and 0.2 for the neat cPAN and GQD-coated cPAN fibres, respectively. A similar Raman spectrum for GQDs, as shown in Fig. 3B, was also observed in our previous study,[73] which confirmed the uniform coating of GQDs on the cPAN fibres.

3.1. Three-electrode electrochemical studies

The supercapacitor studies were performed on the neat cPAN and GQD-coated cPAN electrode for comparison. Platinum, Ag/AgCl and 1 M H_2SO_4 were used as the counter electrode, reference electrode and electrolyte, respectively, in the three-electrode system. Cyclic voltammetry (CV) was performed on neat cPAN and different concentrations of GQDs (0.1 and 0.4 mg) were coated on cPAN as the working electrode. The CV curves were recorded at 10 mV s^{-1}, 25 mV s^{-1}, 50 mV s^{-1}, 75 mV s^{-1} and 100 mV s^{-1} in the potential window of −0.3 V to 0.8 V. The CV of neat cPAN (Fig. 4A) exhibited an almost negligible integrated area, confirming its very low specific capacitance as well as insignificant current and power density values. Alternatively, in the case of the GQD-coated cPAN electrode, a high integrated area was observed, indicating its much higher capacitive behaviour together with high energy and power density compared to the neat cPAN electrode. Noticeably, the 0.1 mg GQD-coated cPAN electrode showed a lower current density compared to the 0.4 mg GQD-coated cPAN electrode. The nonpolar nature of GQDs showed better adhesion with cPAN given that the carbonized PAN fibre also showed nonpolar behaviour. Furthermore, the observed augmentation in surface area (as shown in Fig. S6†) calculated using the BET method resulted in an enhanced capacitive performance.

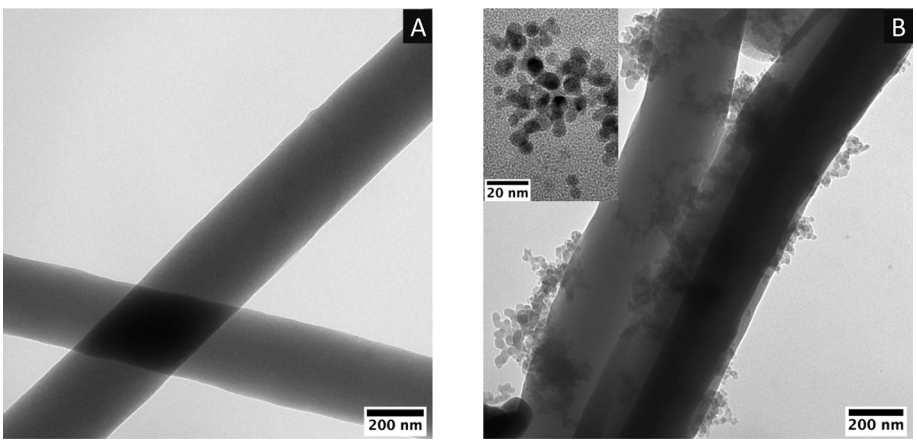

Fig. 1 (A) TEM image of cPAN fibres. (B) 0.4 mg GQD-coated cPAN fibres and high-resolution image of GQDs inserted in the top left corner.

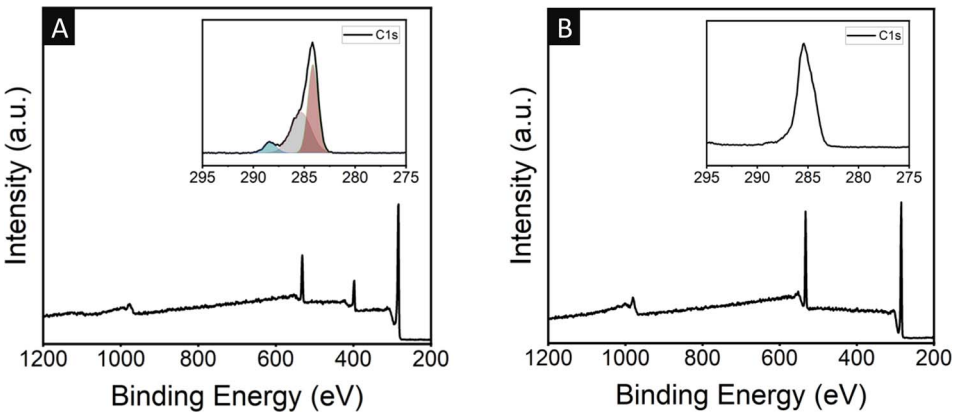

Fig. 2 X-ray photoelectron spectroscopy (XPS) full scan survey of (A) the neat cPAN and (B) 0.4 mg GQD-coated cPAN fabric (high-resolution C 1s spectrum is inserted in the top-right corner).

Fig. S2A and S2B† show that as the scan rate increased from 10 to 100 mV s^{-1}, a slight improvement in the area and shape symmetry was observed. This confirmed the high rate capacitive performance and low internal resistance of the active quantum material.[78,79]

Furthermore, galvanostatic charge–discharge (GCD) experiments were carried out to evaluate the performance of the neat and GQD-coated cPAN electrode at different current densities. For comparison, the GCD of the neat and 0.1 mg GQDs coated cPAN electrodes (Fig. 4B) was recorded in the potential window of −0.3 to 0.8 V at a scan rate of 0.8 mV s^{-1}. The discharge time for the neat cPAN electrode was calculated to be 33 s, while that in the case of the 0.1 mg GQD-coated cPAN electrode was 617 s. The results confirmed that even 0.1 mg of nonpolar GQDs could lead to an exceptional capacitive performance. The discharge time from the GCD profiles was used to calculate the specific areal capacitance values from eqn (1). The specific areal capacitance for the neat cPAN was 24, 15.5, 9.8, 6.4 and 4.4 mF cm^{-2} (and its volumetric capacitance was 12, 7.3, 4.9, 3.1, 2.1 F g^{-1}) at a current density of 0.8, 1.0, 1.2, 1.4, and 1.6 mA cm^{-2}, respectively (Table S1†). Alternatively, the areal capacitance values for the 0.1 mg GQD-coated cPAN electrode were found to be 611.5, 448.7, 291.8, 135.3, and 41.8 mF cm^{-2} (and volumetric capacitance was 291.2, 213.7, 138.9, 64.4 and 19.9 F g^{-1}) at a current density of 0.6, 0.8, 1.0, 1.2, and 2.0 mA cm^{-2}, respectively (Table S2†). In the case of the 0.4 mg GQD-coated cPAN electrode, a maximum areal capacitance of 1883.6 mF cm^{-2} (and volumetric capacitance of 784.9 F g^{-1}) at 2 mA cm^{-2} current density was observed (Table S3†). Thus, a huge jump by 25- and 78-times the specific areal capacitance was observed for the 0.1 mg and 0.4 mg GQD-coated cPAN electrodes, respectively. In contrast, the IR drop increased after increasing the GQD concentration from 0.1 mg to 0.4 in the cPAN electrode (Fig. S3A†).

Fig. 5A shows the GCD profile of the 0.1 mg GQD-coated cPAN with varying current densities of 0.6, 0.8, 1.0, 1.2, and 2.0 mA cm^{-2}. Moreover, a decrease in specific areal capacitance was also seen with an increase in current density for both the neat and 0.1 mg GQD-coated cPAN electrodes, as shown in Fig. 5B. The stability of the electrode plays a crucial role in real field applications. Thus, the capacitance retention capabilities of the 0.1 mg GQD-coated cPAN supercapacitor were tested at a current density of 6 mA cm^{-2}. The regular charge–discharge measurements were performed for 3000 cycles for the evaluation of cyclic stability (Fig. S4†). A good capacitance retention of

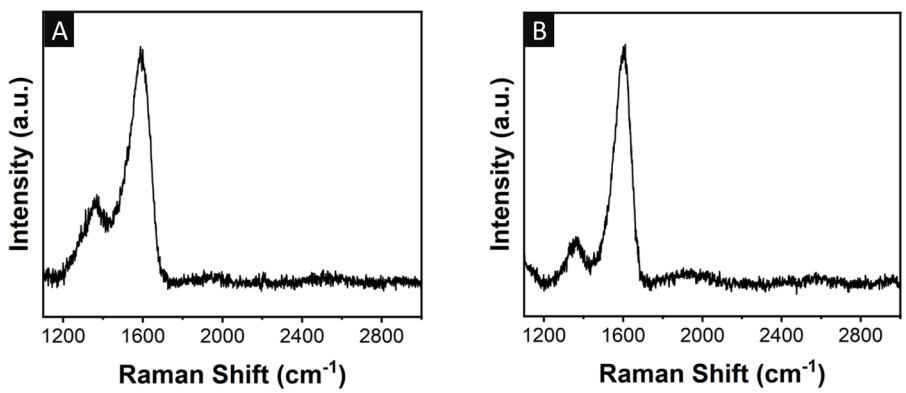

Fig. 3 Raman spectra of (A) neat cPAN and (B) 0.4 mg GQD-coated cPAN fibres.

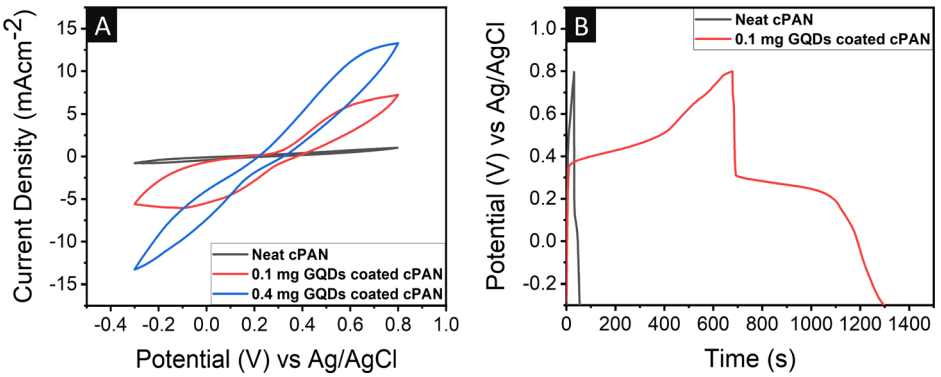

Fig. 4 (A) CV curves collected for neat cPAN and different concentrations of GQD-coated cPAN at a scan rate of 100 mV s^{-1}. (B) GCD curves collected for neat cPAN and 0.1 mg GQD-coated cPAN matrices at a current density of 0.8 mA cm^{-2}.

81.7% was seen even after 3000 continuous charge–discharge cycles.

Electrochemical impedance spectroscopy (EIS) was also performed on the 0.1 mg GQD-coated cPAN electrode to understand its electrochemical kinetics. The EIS measurement was conducted in the frequency range of 100 kHz to 0.1 Hz at an AC signal of 5 mV. The Nyquist plot (Fig. 6A) was comprised of a semi-circle attached with an inclined line, representing the overall resistance of the devices (including the resistance of the electrode, electrolyte, their contact, and charge transfer resistance) and Warburg impedance, respectively. The circuit fit showed the values of 20.3 and 34.1 Ω for equivalent series resistance (R_s) and charge transfer resistance (R_{ct}) respectively, which indicated the good mobility of the electrolyte ions with enhanced charge transfer.[80,81] Also, the high linear slope suggested better ion diffusion throughout the active matrix.

The maximum amount of energy that can be stored and the maximum rate of energy transfer per unit area are the two main factors for any energy device, which decide its market value and are referred to as the energy density and power density, respectively. The energy density and power density values were calculated using eqn (2) and (3), respectively. In the case of the neat cPAN electrode system, the maximum energy density of 4 μW h cm^{-2} with a power density of 440 μW cm^{-2} was observed at a current density of 0.8 mA m^{-2}, as shown in the Ragone plot in Fig. 6B. Interestingly, a jump of around 19 times (75.4 μW h cm^{-2}) was seen in energy density in the case of the 0.1 mg GQD-coated cPAN electrode system with the same power density of 440 μW cm^{-2} and current density of 0.8 mA m^{-2}. The maximum energy density of 102.8 μW h cm^{-2} was calculated at a power density of 330 μW cm^{-2} and current density of 0.6 mA m^{-2}, which was 26 times higher than the maximum power density observed in the neat cPAN electrode system. The capacitance, energy density and power density values of our electrodes were compared with previous studies (Fig. 7A). It was clearly observed that our non-biodegradable plastic waste GQD-coated three-electrode supercapacitor showed good capacitance, energy density and current density values compared to previous studies.

3.2. Two-electrode electrochemical studies

A two-electrode-based coin cell supercapacitor device was also fabricated using 0.1 mg GQD-coated cPAN fabric and its electrochemical analysis was performed. The GQD-coated cPAN, cotton fabric, and neat cPAN were cut into a circular shape with a diameter of 15 mm and used as the cathode, separator and anode, respectively (Fig. 8A). The cathode, anode and separator were all dipped in 1 M H_2SO_4 solution as the electrolyte used in

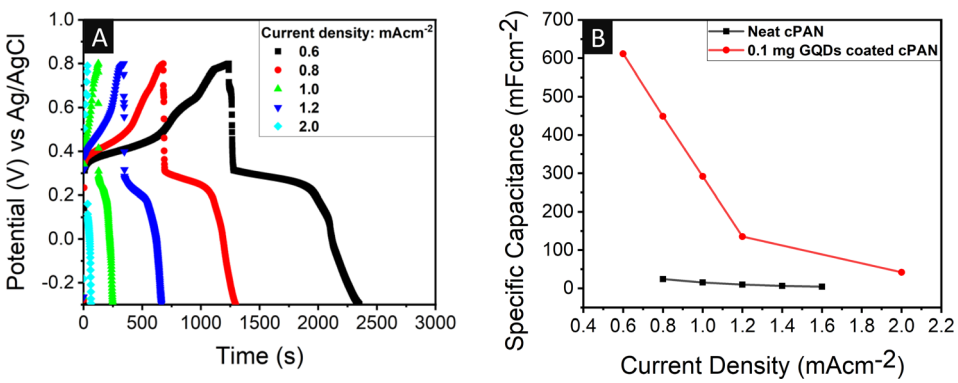

Fig. 5 (A) GCD curves of 0.1 mg GQD-coated cPAN matrices collected at various current densities. (B) Specific capacitance of neat and GQD-coated cPAN matrices at different current densities.

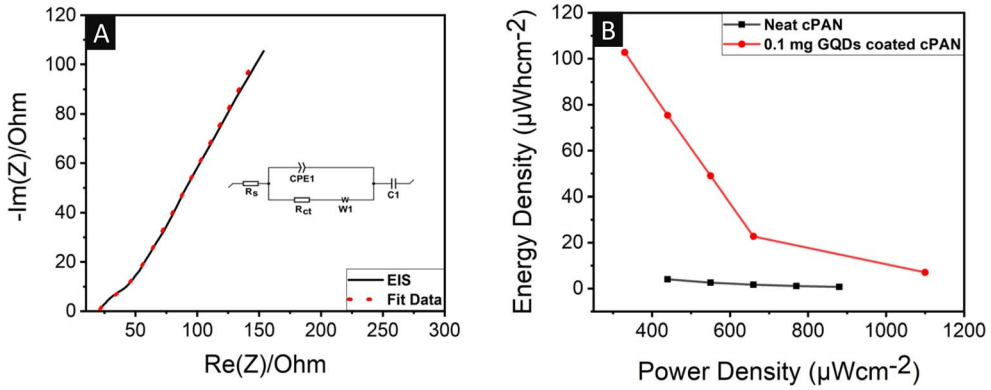

Fig. 6 (A) Nyquist plot of the GQD-coated cPAN matrix with the circuit fit and circuit diagram inserted on the right-hand side. (B) Ragone plot of energy density and power density for neat and GQD-coated cPAN matrices.

the three-electrode system. Subsequently, the whole assembly was packed tightly with the help of a spacer to avoid any unwanted gaps between the electrodes. The CV characteristics were recorded (Fig. 8B) in the same potential window and identical scan rates as the three-electrode system. The integrated area of the GQD-coated two-electrode based supercapacitor was greater than the neat cPAN-based three-electrode system (Fig. S3B†), which further indicated the higher capacitance values of the two-electrode device.

Moreover, the GCD curves were also recorded for the calculation of the actual capacitance values at different current densities, as shown in Fig. 9A. The specific areal capacitance values for the 0.1 mg GQD-coated two-electrode-based system were 59.7, 48.3, 38.7, 30.8 and 5.9 mF cm^{-2} (and volumetric capacitance was 28.4, 22.9, 18.4, 14.7 and 2.8 F g^{-1}) at the current density of 0.4, 0.6, 0.8, 1.0, and 2.0 mA cm^{-2}, respectively (Table S4†). The areal capacitance of the two-electrode supercapacitor device for the different materials is shown in Fig. 7B. The areal capacitance of GQDs obtained from non-biodegradable plastic waste in the present work was significantly higher than that in the previously reported studies. EIS was also performed on the 0.1 mg GQD-coated two-electrode system in the frequency range of 100 kHz to 0.1 Hz at an AC signal of 5 mV. The Nyquist plot of the two-electrode device (Fig. 9B) consisted of a larger area semi-circle compared to that observed in the three-electrode system attached with inclined line. This larger area semi-circle indicated the higher resistance in the two-electrode device compared to the three-electrode system because of the restricted mobility of charge usually seen in three-electrode setups. The equivalent series resistance and charge transfer resistance were also calculated using the relevant circuit fit. The R_s and R_{ct} values were found to be 2.2 and 119.3 Ω. The comparison of the R_s and R_{ct} values with that of the three-electrode system reflected that the R_s value decreased by 9.2 times, but on the contrary the R_{ct} value increased by 3.5 times.

As shown in Fig. 10A, GCD was also performed for 3000 regular charge–discharge cycles to evaluate the device stability

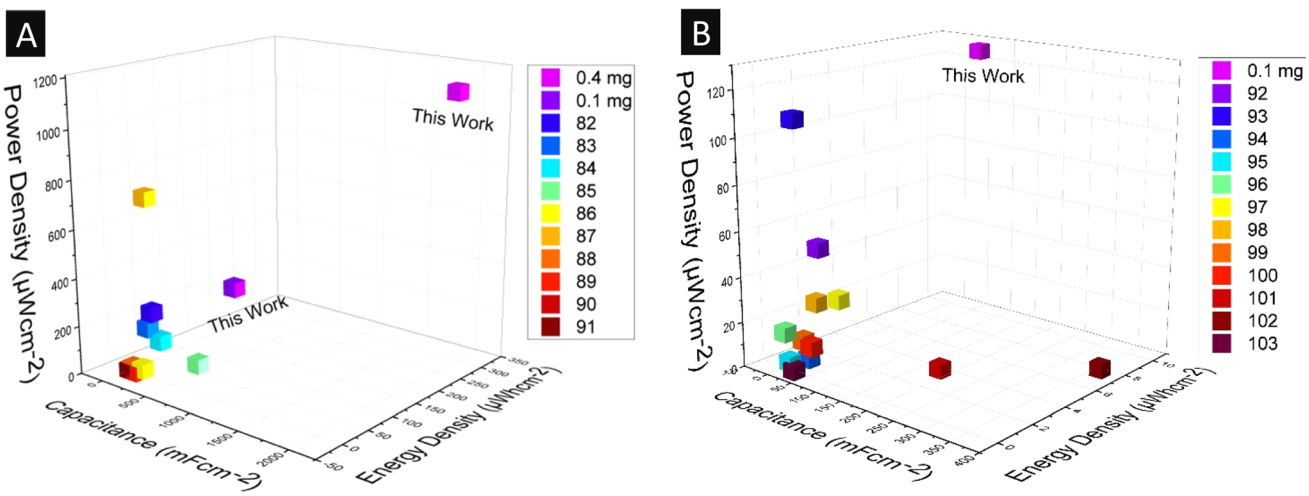

Fig. 7 (A) Three-electrode system areal capacitance, energy density and power density literature survey[82–91] compared with 0.4 mg and 0.1 mg GQD-coated cPAN electrodes. (B) Literature survey of areal capacitance, energy density and power density of the two-electrode system[92–103] compared with the 0.1 mg GQD-coated coin cell fabricated in this work.

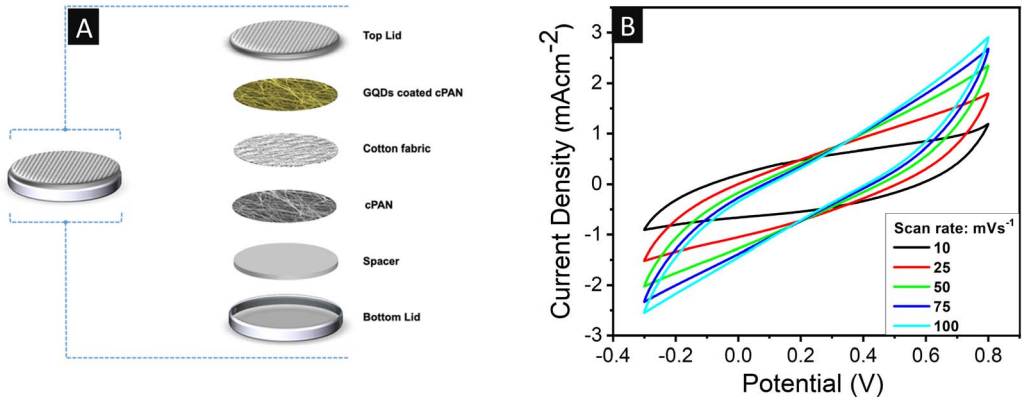

Fig. 8 (A) Graphical representation of the coin cell-based two-electrode supercapacitor. (B) CV curves of 0.1 mg GQD-coated cPAN matrices collected at various scan rates.

of the two-electrode device. After all the charge–discharge cycles, a good capacitance retention of 98.7% was observed, indicating that the two-electrode supercapacitor was stable. A maximum areal energy density value of 10 μW h cm^{-2} at a power density of 125 μW cm^{-2} was observed at a current density of 0.4 mA m^{-2} (Fig. 10B). Furthermore, as the current density increased, the energy density decreased, while the power density increased. The maximum power density of 625 μW cm^{-2} was calculated at 1 μW h cm^{-2} and 2 mA m^{-2} energy density and current density, respectively. The energy density and power density values of the two-electrode system for different materials are shown in Fig. 7B. It can be found that the energy density of 10 μW h cm^{-2} at a power density of 125 μW cm^{-2} established a significant improvement compared to the values in the literature.

4. Conclusion

A feasible approach to convert hazardous, non-biodegradable plastic waste into a value-added product was reported herein. GQDs of controlled dimensions and nonpolar properties were reproducibly generated *via* the microwave-assisted pyrolysis of Styrofoam waste without using any corrosive acids or bases. Subsequently, a supercapacitor was fabricated based on the as-obtained GQDs by depositing the GQDs on a cPAN matrix and the supercapacitance performance of three- and two-electrode-based systems was evaluated. The three-electrode system based on neat cPAN showed a specific areal capacitance value of 24 mF cm^{-2}, while in the case of the GQD-coated cPAN three-electrode, the maximum capacitance values of 611 mF cm^{-2} and 1883 mF cm^{-2} were obtained with a 0.1 mg and 0.4 mg concentration of GQDs, respectively. Good energy density and power density values were seen at 102 μW h cm^{-2} (0.1 mg GQD) and 330 μW cm^{-2} (0.4 mg GQD), respectively, with capacitance retention during 3000 charge–discharge cycles. A maximum capacitance value of 78 times higher than the cPAN electrode was seen after coating the nonpolar GQDs. Alternatively, the two-electrode system exhibited the maximum capacitance of 59.7 mF cm^{-2} at the current density of 0.4 mA cm^{-2}. Also, the two-electrode-based coin cell supercapacitor outperformed the neat cPAN three-electrode system in terms of areal capacitance and energy density values. GQDs coated on the cPAN electrode clearly showed better adhesion because of their nonpolar nature and defect-free sp^2 hybridization, which contributed to

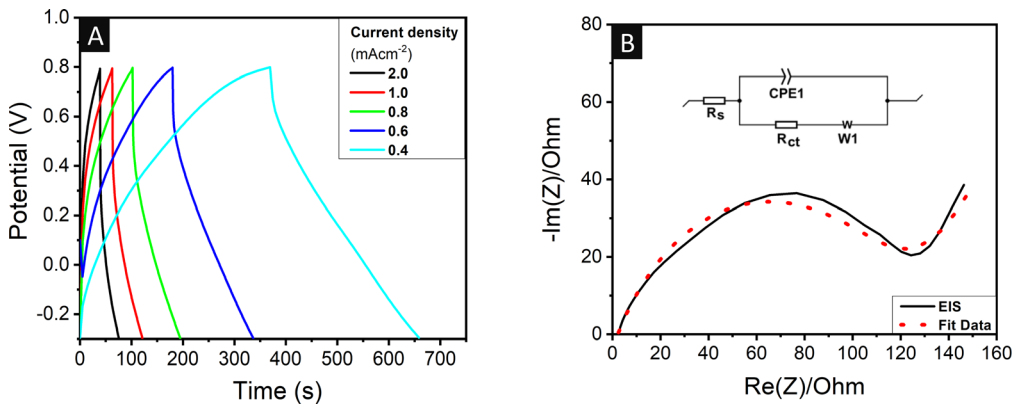

Fig. 9 Two-electrode system (A) GCD curves of 0.1 mg GQD-coated cPAN matrix collected at various current densities. (B) Two-electrode Nyquist plot of 0.1 mg GQD-coated cPAN matrix with circuit fit and the circuit diagram inserted in the top centre.

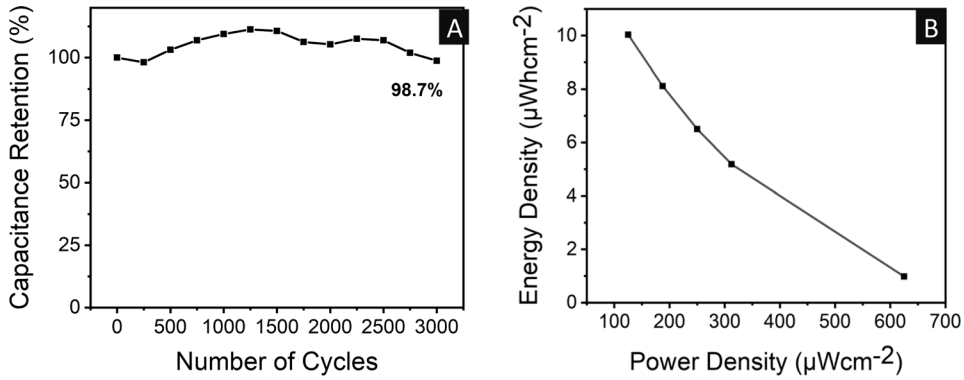

Fig. 10 (A) Capacitance retention of 0.1 mg GQD-coated cPAN matrix for 3000 cycles in the two-electrode supercapacitor. (B) Ragone plot of energy density and power density for the 0.1 mg GQD-coated two-electrode system.

the overall conductivity enhancement of the electrode. The better adhesion and higher conductivity of GQDs led to a very high specific areal capacitance. The developed approach can be further explored to realize the sustainable idea of non-biodegradable plastic waste utilization in the field of energy storage materials and provide an unforeseen opportunity to address the current energy and waste management demands.

Author contrubution

Dheeraj Kumar: methodology, data curation, formal analysis, investigation, writing – original draft. Ekta Vashishth: data curation, formal analysis. Sweety Rani: data curation, formal analysis, writing – review & editing. Advitiya Kumar: data curation, formal analysis. Bhanu Nandan: resources, writing – review & editing. Supreet Singh Bahga: resources, writing – review & editing. Rajiv K. Srivastava: conceptualization, validation, supervision, project administration, funding acquisition writing – review & editing.

Conflicts of interest

There are no conflicts to declare.

Acknowledgements

Authors gratefully acknowledge the support provided by the Central Research Facility (CRF, IIT Delhi) and Indian Institute of Technology, Delhi to perform this research work.

References

1 Z. Yu, L. Tetard, L. Zhai and J. Thomas, Supercapacitor electrode materials: nanostructures from 0 to 3 dimensions, *Energy Environ. Sci.*, 2015, **8**, 702–730.
2 W. Raza, F. Ali, N. Raza, Y. Luo, K.-H. Kim, J. Yang, *et al.*, Recent advancements in supercapacitor technology, *Nano Energy*, 2018, **52**, 441–473.
3 K. S. Kumar, N. Choudhary, Y. Jung and J. Thomas, Recent Advances in Two-Dimensional Nanomaterials for Supercapacitor Electrode Applications, *ACS Energy Lett.*, 2018, **3**, 482–495.
4 B. Qi, X. Hong, Y. Jiang, J. Shi, M. Zhang, W. Yan, *et al.*, A Review on Engineering Design for Enhancing Interfacial Contact in Solid-State Lithium–Sulfur Batteries, *Nano-Micro Lett.*, 2024, **16**, 71.
5 B. Cao, S. Gao, Y. Ma, D. Zhang, Z. Guo, M. Du, *et al.*, Biomass-derived carbon-sulfur hybrids boosting electrochemical kinetics to achieve high potassium storage performance, *J. Colloid Interface Sci.*, 2024, **661**, 598–605.
6 K. Wang, C. Lu, Q. Ren, W. Zhang, H. Huang, J. Zhang, *et al.*, Three-dimensional laminated carbon-sulfur composite cathodes derived from Trichoderma spores for lithium-sulfur batteries, *J. Electroanal. Chem.*, 2023, **928**, 117017.
7 D. Zhong, K. Wang, Y. Zuo, M. Wei, J. Xiong, H. Wang, *et al.*, Metal–air batteries for powering robots, *J. Mater. Chem. A*, 2023, **11**, 25115–25135.
8 P. R. Kharangarh, N. M. Ravindra, G. Singh and S. Umapathy, Synthesis of luminescent graphene quantum dots from biomass waste materials for energy-related applications—An overview, *Energy Storage*, 2022, **5**, e369.
9 Y. Jin, Y. Wang, P.-G. Ren, B. Zhang, Z. Zhao, X. Hou, *et al.*, Recent advances of carbon dots based emerging materials for supercapacitors applications, *J. Energy Storage*, 2024, **85**, 111118.
10 H. Cho, G. Bae and B. H. Hong, Engineering functionalization and properties of graphene quantum dots (GQDs) with controllable synthesis for energy and display applications, *Nanoscale*, 2024, **16**, 3347–3378.
11 T. Jiang, Y. Wang and G. Z. Chen, Electrochemistry of Titanium Carbide MXenes in Supercapacitor, *Small Methods*, 2023, **7**, 2201724.
12 Y. A. Kumar, C. J. Raorane, H. H. Hegazy, T. Ramachandran, S. C. Kim and M. Moniruzzaman, 2D MXene-based supercapacitors: A promising path towards high-performance energy storage, *J. Energy Storage*, 2023, **72**, 108433.

13 I. Mubeen, S. Shah, E. Pervaiz and W. Miran, The promising frontier for next-generation energy storage and clean energy production: A review on synthesis and applications of MXenes, *Mater. Sci. Energy Technol.*, 2024, **7**, 180–194.
14 Y. Wang, L. Zhang, H. Hou, W. Xu, G. Duan, S. He, *et al.*, Recent progress in carbon-based materials for supercapacitor electrodes: a review, *J. Mater. Sci.*, 2020, **56**, 173–200.
15 M. Saleem, F. Ahmad, M. Fatima, A. Shahzad, M. S. Javed, S. Atiq, *et al.*, Exploring new frontiers in supercapacitor electrodes through MOF advancements, *J. Energy Storage*, 2024, **76**, 109822.
16 R. Patil, N. Kumar, B. Matsagar, K. C. W. Wu, R. R. Salunkhe and S. Dutta, An improved Hummers method derived graphene oxide wrapped ZIF-8 polyhedron derived porous heterostructure for symmetric supercapacitor performance, *RSC Sustain.*, 2024, **2**, 233–238.
17 S. Wustoni, D. Ohayon, A. Hermawan, A. Nuruddin, S. Inal, Y. S. Indartono, *et al.*, Material Design and Characterization of Conducting Polymer-Based Supercapacitors, *Polym. Rev.*, 2023, **64**, 192–250.
18 J. Hao, B. Wang, H. Xu, J. Du, C. Wu, W. Qin, *et al.*, Interfacial regulation of biomass-derived carbon towards high-performance supercapacitor, *J. Energy Storage*, 2024, **86**, 111301.
19 H. Li, H. Yang, H. Sun, Y. Huang, P. An, Y. Yunhua, *et al.*, A manganese oxide/biomass porous carbon composite for high-performance supercapacitor electrodes, *Electrochim. Acta*, 2024, **473**, 143514.
20 B. Liu, Y. Ye, M. Yang, Y. Liu, H. Chen, H. Li, *et al.*, All-in-one Biomass-Based Flexible Supercapacitors with High Rate Performance and High Energy Density, *Adv. Funct. Mater.*, 2023, **34**, 2310534.
21 Y. Wang, T. Xu, K. Liu, M. Zhang, X. Cai and C. Si, Biomass-based materials for advanced supercapacitor: principles, progress, and perspectives, *Aggregate*, 2023, **5**, e428.
22 M. Al-Enizi A, A. Nafady, N. B. Alanazi, M. M. Abdulhameed and S. F. Shaikh, Waste polyethylene terephthalate plastic derived Zr-MOF for high performance supercapacitor applications, *Chemosphere*, 2024, **350**, 141080.
23 X. Li, G. Wu, Z. Zhang, J. Yao, K. Song and S. Komarneni, Plastic wastes-derived electro-spun nanofiber/MnO2 nanocomposite for flexible supercapacitor application, *Polymer*, 2024, **292**, 126623.
24 N. Choudhary, C. Li, J. Moore, N. Nagaiah, L. Zhai, Y. Jung, *et al.*, Asymmetric Supercapacitor Electrodes and Devices, *Adv. Mater.*, 2017, **29**, 1605336.
25 N. Arsalani, L. S. Ghadimi, I. Ahadzadeh, A. G. Tabrizi and T. Nann, Green Synthesized Carbon Quantum Dots/Cobalt Sulfide Nanocomposite as Efficient Electrode Material for Supercapacitors, *Energy Fuels*, 2021, **35**, 9635–9645.
26 A. M. Al-Enizi, M. Ubaidullah and D. Kumar, Carbon quantum dots (CQDs)/Ce doped NiO nanocomposite for high performance supercapacitor, *Mater. Today Commun.*, 2021, **27**, 102340.
27 M. Naushad, T. Ahamad, M. Ubaidullah, J. Ahmed, A. A. Ghafar, K. M. Al-Sheetan, *et al.*, Nitrogen-doped carbon quantum dots (N-CQDs)/Co3O4 nanocomposite for high performance supercapacitor, *J. King Saud Univ. Sci.*, 2021, **33**, 101252.
28 Z. Ji, D. Ma, W. Dai, K. Liu, X. Shen, G. Zhu, *et al.*, Anchoring nitrogen-doped carbon quantum dots on nickel carbonate hydroxide nanosheets for hybrid supercapacitor applications, *J. Colloid Interface Sci.*, 2021, **590**, 614–621.
29 K. Kakaei, S. Khodadoost, M. Gholipour and N. Shouraei, Core-shell polyaniline functionalized carbon quantum dots for supercapacitor, *J. Phys. Chem. Solids*, 2021, **148**, 109753.
30 K. Yang, Z. Luo, D. Shu, F. Yi, Z. Zhu and A. Gao, Design of few-layered 1T-MoS2 by supramolecular-assisted assembly with N-doped carbon quantum dots for supercapacitor, *J. Electroanal. Chem.*, 2022, **908**, 116093.
31 W. Luo, W. Chen, H. Quan, Z.-X. Zhang, Y. Zeng, Y. Wang, *et al.*, Strongly coupled carbon quantum dots/NiCo-LDHs nanosheets on carbon cloth as electrode for high performance flexible supercapacitors, *Appl. Surf. Sci.*, 2022, **591**, 153161.
32 M. S. Kumar, Y. Y. K, P. Das, S. Malik, N. K. Kothurkar and S. K. Batabyal, Urea-mediated synthesized carbon quantum dots to tune the electrochemical performance of polyaniline nanorods for supercapacitor device, *J. Sci.: Adv. Mater. Devices*, 2022, **7**, 100403.
33 M. R. Pallavolu, N. Gaddam, A. N. Banerjee, R. R. Nallapureddy and S. W. Joo, Superior energy-power performance of N-doped carbon nano-onions-based asymmetric and symmetric supercapacitor devices, *Int. J. Energy Res.*, 2021, **46**, 1234–1249.
34 M. Majumder, A. K. Thakur, M. Bhushan and D. Mohapatra, Polyaniline integration and interrogation on carbon nano-onions empowered supercapacitors, *Electrochim. Acta*, 2021, **370**, 137659.
35 E. Sohouli, K. Adib, B. Maddah and M. Najafi, Manganese dioxide/cobalt tungstate/nitrogen-doped carbon nano-onions nanocomposite as new supercapacitor electrode, *Ceram. Int.*, 2022, **48**, 295–303.
36 G. Dhakal, D. Mohapatra, T. L. Tamang, M. Lee, Y. R. Lee and J.-J. Shim, Redox-additive electrolyte–driven enhancement of the electrochemical energy storage performance of asymmetric Co3O4//carbon nano-onions supercapacitors, *Energy*, 2021, **218**, 119436.
37 J. Lei, J. Liu, N. Tang, H. Han, Z. Li, K. Li, *et al.*, Novel Gram-Scale Synthesis of Carbon Nano-Onions from Heavy Oil for Supercapacitors, *Adv. Mater. Interfaces*, 2021, **8**, 2101208.
38 L. Fornasini, S. Scaravonati, G. Magnani, A. Morenghi, M. Sidoli, D. Bersani, *et al.*, In situ decoration of laser-scribed graphene with TiO2 nanoparticles for scalable high-performance micro-supercapacitors, *Carbon*, 2021, **176**, 296–306.
39 M. Reina, A. Scalia, G. Auxilia, M. Fontana, F. Bella, S. Ferrero, *et al.*, Boosting Electric Double Layer

Capacitance in Laser-Induced Graphene-Based Supercapacitors, *Adv. Sustain. Syst.*, 2021, **6**, 2100228.
40 N. A. Salleh, S. Kheawhom and A. A. Mohamad, Chitosan as biopolymer binder for graphene in supercapacitor electrode, *Results Phys.*, 2021, **25**, 104244.
41 M. Khandelwal, C. V. Tran, J. Lee and J. B. In, Nitrogen and boron co-doped densified laser-induced graphene for supercapacitor applications, *Chem. Eng. J.*, 2022, **428**, 131119.
42 P. Ponmani, J. Bahadur, C. Tewari, D. K. Gupta, U. Kalita, P. Jegadeesan, *et al.*, Polyaniline modified waste-derived graphene/sulfur nanocomposite cathode for lithium–sulfur batteries, *J. Polym. Sci.*, 2023, 1–14.
43 C. Chen, M. Zhao, Y. Cai, G. Zhao, Y. Xie, L. Zhang, *et al.*, Scalable synthesis of strutted nitrogen doped hierarchical porous carbon nanosheets for supercapacitors with both high gravimetric and volumetric performances, *Carbon*, 2021, **179**, 458–468.
44 K. Chen, S. Weng, J. Lu, J. Gu, G. Chen, O. Hu, *et al.*, Facile synthesis of chitosan derived heteroatoms-doped hierarchical porous carbon for supercapacitors, *Microporous Mesoporous Mater.*, 2021, **320**, 111106.
45 X. Liang, R. Liu and X. Wu, Biomass waste derived functionalized hierarchical porous carbon with high gravimetric and volumetric capacitances for supercapacitors, *Microporous Mesoporous Mater.*, 2021, **310**, 110659.
46 F. Ran, X. Yang, X. Xu, S. Li, Y. Liu and L. Shao, Green activation of sustainable resources to synthesize nitrogen-doped oxygen-riched porous carbon nanosheets towards high-performance supercapacitor, *Chem. Eng. J.*, 2021, **412**, 128673.
47 J. Cheng, Z. Lu, X. Zhao, X. Chen and Y. Liu, Green needle coke-derived porous carbon for high-performance symmetric supercapacitor, *J. Power Sources*, 2021, **494**, 229770.
48 C. Zhao, Y. Ding, Y. Huang, N. Li, Y. Hu and C. Zhao, Soybean root-derived N, O co-doped hierarchical porous carbon for supercapacitors, *Appl. Surf. Sci.*, 2021, **555**, 149726.
49 R. Wang, X. Li, Z. Nie, Y. Zhao and H. Wang, Metal/Metal Oxide Nanoparticles-Composited Porous Carbon for High-Performance Supercapacitors, *J. Energy Storage*, 2021, **38**, 102479.
50 X. Chu, F. Meng, T. Deng and W. Zhang, Metal organic framework derived porous carbon materials excel as an excellent platform for high-performance packaged supercapacitors, *Nanoscale*, 2021, **13**, 5570–5593.
51 M. Miah, S. Bhattacharya, A. Gupta and S. K. Saha, Origin of high storage capacity in N-doped graphene quantum dots, *Electrochim. Acta*, 2016, **222**, 709–716.
52 S. Zhang, L. Sui, H. Dong, W. He, L. Dong and L. Yu, High-Performance Supercapacitor of Graphene Quantum Dots with Uniform Sizes, *ACS Appl. Mater. Interfaces*, 2018, **10**, 12983–12991.
53 R. Tjandra, W. Liu, M. Zhang and A. Yu, All-carbon flexible supercapacitors based on electrophoretic deposition of graphene quantum dots on carbon cloth, *J. Power Sources*, 2019, **438**, 227009.
54 A. Singh, S. Kumar and A. K. Ojha, Charcoal derived graphene quantum dots for flexible supercapacitor oriented applications, *New J. Chem.*, 2020, **44**, 11085–11091.
55 W. Tian, J. Zhu, Y. Dong, J. Zhao, J. Li, N. Guo, *et al.*, Micelle-induced assembly of graphene quantum dots into conductive porous carbon for high rate supercapacitor electrodes at high mass loadings, *Carbon*, 2020, **161**, 89–96.
56 S. Zhang, J. Zhu, Y. Qing, L. Wang, J. Zhao, J. Li, *et al.*, Ultramicroporous Carbons Puzzled by Graphene Quantum Dots: Integrated High Gravimetric, Volumetric, and Areal Capacitances for Supercapacitors, *Adv. Funct. Mater.*, 2018, **28**, 1805898.
57 Z. Ouyang, Y. Lei, Y. Chen, Z. Zhang, Z. Jiang, J. Hu, *et al.*, Preparation and Specific Capacitance Properties of Sulfur, Nitrogen Co-Doped Graphene Quantum Dots, *Nanoscale Res. Lett.*, 2019, **14**, 219.
58 L. Xu, C. Cheng, C. Yao and X. Jin, Flexible supercapacitor electrode based on lignosulfonate-derived graphene quantum dots/graphene hydrogel, *Org. Electron.*, 2020, **78**, 105407.
59 H. Kuzhandaivel, S. Manickam, S. K. Balasingam, M. C. Franklin, H.-J. Kim and K. S. Nallathambi, Sulfur and nitrogen-doped graphene quantum dots/PANI nanocomposites for supercapacitors, *New J. Chem.*, 2021, **45**, 4101–4110.
60 M. T. Dejpasand, S. Sharifi, E. Saievar-Iranizad, A. Yazdani and K. Rahimi, Boron- and nitrogen-doped graphene quantum dots with enhanced supercapacitance, *J. Energy Storage*, 2021, **42**, 103103.
61 V. Gayathri, P. I. John, K. Ramachandran, S. Karazhanov and M. C. Raja, Graphene Quantum Dots Embedded in NiCo2S4/MWCNT Nanocomposite as a Promising Candidate for Supercapacitors and I3– Reduction in Dye-Sensitized Solar Cells, *Energy Fuels*, 2021, **35**, 13360–13369.
62 M. Ashourdan, A. Semnani, F. Hasanpour and S. E. Moosavifard, Synthesis of CuMnO2/graphene quantum dot nanocomposites as novel electrode materials for high performance supercapacitors, *J. Energy Storage*, 2021, **36**, 102449.
63 T. A. Raja, P. Vickraman, A. S. Justin and B. J. Reddy, Ultrasonicated graphene quantum dots dispersoid zinc ammonium phosphate hybrid electrode for supercapacitor applications, *J. Mater. Sci.: Mater. Electron.*, 2022, **33**, 7079–7098.
64 Z. Li, X. Wang, M. Xu, Z. Yin and J. Zhao, Facile strategy for preparing the composite of MoS2 microspheres and N/S dual-doped graphene stabilized by graphene quantum dots for all-solid-state asymmetric supercapacitor, *J. Alloys Compd.*, 2022, **894**, 162492.
65 J. Wei, X. Zhang, Y. Sheng, J. Shen, P. Huang, S. Guo, *et al.*, Simple one-step synthesis of water-soluble fluorescent carbon dots from waste paper, *New J. Chem.*, 2014, **38**, 906.
66 A. Kumari, A. Kumar, S. K. Sahu and S. Kumar, Synthesis of green fluorescent carbon quantum dots using waste

polyolefins residue for Cu2+ ion sensing and live cell imaging, *Sens. Actuators, B*, 2018, **254**, 197–205.

67 Y. Hu, J. Yang, J. Tian, L. Jia and J.-S. Yu, Green and size-controllable synthesis of photoluminescent carbon nanoparticles from waste plastic bags, *RSC Adv.*, 2014, **4**, 47169–47176.

68 S. Y. Park, H. U. Lee, E. S. Park, S. C. Lee, J.-W. Lee, S. W. Jeong, *et al.*, Photoluminescent Green Carbon Nanodots from Food-Waste-Derived Sources: Large-Scale Synthesis, Properties, and Biomedical Applications, *ACS Appl. Mater. Interfaces*, 2014, **6**, 3365–3370.

69 S. T and D. RS, Green synthesis of highly fluorescent carbon quantum dots from sugarcane bagasse pulp, *Appl. Surf. Sci.*, 2016, **390**, 435–443.

70 A. Prasannan and T. Imae, One-Pot Synthesis of Fluorescent Carbon Dots from Orange Waste Peels, *Ind. Eng. Chem. Res.*, 2013, **52**, 15673–15678.

71 A. Tyagi, K. M. Tripathi, N. Singh, S. Choudhary and R. K. Gupta, Green synthesis of carbon quantum dots from lemon peel waste: applications in sensing and photocatalysis, *RSC Adv.*, 2016, **6**, 72423–72432.

72 N.-J. Kuo, Y.-S. Chen, C.-W. Wu, C.-Y. Huang, Y.-H. Chan and I.-W. P. Chen, One-Pot Synthesis of Hydrophilic and Hydrophobic N-Doped Graphene Quantum Dots via Exfoliating and Disintegrating Graphite Flakes, *Sci. Rep.*, 2016, **6**, 30426.

73 D. Kumar, S. Rani, B. Nandan and R. K. Srivastava, Nonpolar Graphene Quantum Dot-Based Hydrophobic Coating from Microwave-Assisted Treatment of Styrofoam Waste, *ACS Sustain. Chem. Eng.*, 2022, **10**, 1070–1077.

74 G. Y. Baek, H. S. Lee, J.-M. Jung, I.-T. Hwang, J. Shin, C.-H. Jung, *et al.*, Preparation of conductive carbon films from polyacrylonitrile/graphene oxide composite films by thermal treatment, *J. Ind. Eng. Chem.*, 2018, **58**, 87–91.

75 G. Wu, C. Lu, X. Wu, S. Zhang, F. He and L. Ling, X-ray photoelectron spectroscopy investigation into thermal degradation and stabilization of polyacrylonitrile fibers, *J. Appl. Polym. Sci.*, 2004, **94**, 1705–1709.

76 H. Wang, Y. Wang, X. Cao, M. Feng and G. Lan, Vibrational properties of graphene and graphene layers, *J. Raman Spectrosc.*, 2009, **40**, 1791–1796.

77 S. Kim, D. Hee Shin, C. Oh Kim, S. Seok Kang, J. S. Sin, S.-H. Choi, *et al.*, Size-dependence of Raman scattering from graphene quantum dots: Interplay between shape and thickness, *Appl. Phys. Lett.*, 2013, **102**, 053108.

78 D. Wei, L. Grande, V. Chundi, R. White, C. Bower, P. Andrew, *et al.*, Graphene from electrochemical exfoliation and its direct applications in enhanced energy storage devices, *Chem. Commun.*, 2012, **48**, 1239–1241.

79 X. Jian, H. Yang, J. Li, E. Zhang, L. Cao and Z. Liang, Flexible all-solid-state high-performance supercapacitor based on electrochemically synthesized carbon quantum dots/polypyrrole composite electrode, *Electrochim. Acta*, 2017, **228**, 483–493.

80 K. Ghosh and S. K. Srivastava, Enhanced Supercapacitor Performance and Electromagnetic Interference Shielding Effectiveness of CuS Quantum Dots Grown on Reduced Graphene Oxide Sheets, *ACS Omega*, 2021, **6**, 4582–4596.

81 M. Vandana, H. Vijeth, S. P. Ashokkumar and H. Devendrappa, Graphene quantum dots doped conducting polymer nanocomposite for high performance supercapacitor application, *Int. J. Nanotechnol.*, 2021, **18**, 494.

82 K. Li, X. Liu, S. Chen, W. Pan and J. Zhang, A flexible solid-state supercapacitor based on graphene/polyaniline paper electrodes, *J. Energy Chem.*, 2019, **32**, 166–173.

83 W. Wang, O. Sadak, J. Guan and S. Gunasekaran, Facile synthesis of graphene paper/polypyrrole nanocomposite as electrode for flexible solid-state supercapacitor, *J. Energy Storage*, 2020, **30**, 101533.

84 MdH. Ahmad, R. B. Alam, A. Ul-hamid, S. F. U. Farhad and M. R. Islam, Hydrothermal synthesis of Co3O4 nanoparticles decorated three dimensional MoS2 nanoflower for exceptionally stable supercapacitor electrode with improved capacitive performance, *J. Energy Storage*, 2022, **47**, 103551.

85 W. Wang, Y. Yang, Z. Chen, Z. Deng, L. Fan, W. Guo, *et al.*, High-performance yarn supercapacitor based on directly twisted carbon nanotube@bacterial cellulose membrane, *Cellulose*, 2020, **27**, 7649–7661.

86 W. Chen, D. Zhang, K. Yang, M. Luo, P. Yang and X. Zhou, Mxene (Ti3C2T)/cellulose nanofiber/porous carbon film as free-standing electrode for ultrathin and flexible supercapacitors, *Chem. Eng. J.*, 2021, **413**, 127524.

87 B. Patil, S. Ahn, C. Park, H. Song, Y. Jeong and H. Ahn, Simple and novel strategy to fabricate ultra-thin, lightweight, stackable solid-state supercapacitors based on MnO2-incorporated CNT-web paper, *Energy*, 2018, **142**, 608–616.

88 H. Wei, J. Zhu, S. Wu, S. Wei and Z. Guo, Electrochromic polyaniline/graphite oxide nanocomposites with endured electrochemical energy storage, *Polymer*, 2013, **54**, 1820–1831.

89 K. Qi, R. Hou, S. Zaman, Y. Qiu, B. Y. Xia and H. Duan, Construction of Metal–Organic Framework/Conductive Polymer Hybrid for All-Solid-State Fabric Supercapacitor, *ACS Appl. Mater. Interfaces*, 2018, **10**, 18021–18028.

90 K. Qi, R. Hou, S. Zaman, Y. Qiu, B. Y. Xia and H. Duan, Construction of Metal–Organic Framework/Conductive Polymer Hybrid for All-Solid-State Fabric Supercapacitor, *ACS Appl. Mater. Interfaces*, 2018, **10**, 18021–18028.

91 G. Gou, F. Huang, M. Jiang, J. Li and Z. Zhou, Hierarchical porous carbon electrode materials for supercapacitor developed from wheat straw cellulosic foam, *Renewable Energy*, 2020, **149**, 208–216.

92 S. Sharma, R. Adalati, M. Sharma, S. Jindal, A. Kumar, G. Malik, *et al.*, Single-step fabrication of di-titanium nitride thin-film flexible and biocompatible supercapacitor, *Ceram. Int.*, 2022, **48**, 34678–34687.

93 S. A. Adewinbi, R. A. Busari, L. O. Animasahun, E. Omotoso and B. A. Taleatu, Effective pseudocapacitive performance of binder free transparent α-V2O5 thin film electrode:

Electrochemical and some surface probing, *Phys. B*, 2021, **621**, 413260.

94 M. Asghar, S. A. Zahra, Z. Khan, M. Ahmed, F. Nasir, M. Iqbal, *et al.*, Laser-Assisted Fabrication of Nanostructured Substrate Supported Electrodes for Highly Active Supercapacitors, *Front Mater.*, 2020, **7**, 179.

95 Y. Bencheikh, A. Addad, Y. Coffinier, U. Kumar, P. Roussel, S. Szunerits, *et al.*, Silicon nanowire-hydrogenated TiO2 core-shell arrays for stable electrochemical micro-capacitors, *Electrochim. Acta*, 2021, **396**, 139198.

96 Z. Pan, Y.-Y. Zhou, Y. Zhang, W.-T. Jiang and G. Y. Zhang, Fabrication and Characterization of Planar on-Chip Micro-Supercapacitors Based on Nitrogen and Oxygen Co-Doped Graphene Quantum Dots by Modified Liquid-Air Interface Self-Assembly Method, *Integrated Ferroelectrics*, 2022, **227**, 89–97.

97 B. Nie, X. Li, J. Shao, C. Li, P. Sun, Y. Wang, *et al.*, Scalable fabrication of high-performance micro-supercapacitors by embedding thick interdigital microelectrodes into microcavities, *Nanoscale*, 2019, **11**, 19772–19782.

98 K. Parida, V. Bhavanasi, V. Kumar, J. Wang and P. S. Lee, Fast charging self-powered electric double layer capacitor, *J. Power Sources*, 2017, **342**, 70–78.

99 W. Yu, B. Q. Li, S. Ding and H. Liu, 3D printing of interdigitated electrode for all-solid-state microsupercapacitors, *J. Micromech. Microeng.*, 2018, **28**, 105014.

100 C. Zhang, L. McKeon, M. P. Kremer, S.-H. Park, O. Ronan, A. Seral-Ascaso, *et al.*, Additive-free MXene inks and direct printing of micro-supercapacitors, *Nat. Commun.*, 2019, **10**, 1795.

101 L. Kou, T. Huang, B. Zheng, Y. Han, X. Zhao, K. Gopalsamy, *et al.*, Coaxial wet-spun yarn supercapacitors for high-energy density and safe wearable electronics, *Nat. Commun.*, 2014, **5**, 3754.

102 X. Zheng, L. Yao, Y. Qiu, S. Wang and K. Zhang, Core–Sheath Porous Polyaniline Nanorods/Graphene Fiber-Shaped Supercapacitors with High Specific Capacitance and Rate Capability, *ACS Appl. Energy Mater.*, 2019, **2**, 4335–4344.

103 S. Nayak, A. Soam, J. Nanda, C. Mahender, M. Singh, D. Mohapatra, *et al.*, Sol–gel synthesized BiFeO3–Graphene nanocomposite as efficient electrode for supercapacitor application, *J. Mater. Sci.: Mater. Electron.*, 2018, **29**, 9361–9368.